Modeling the G-Protein Signaling of the Retina with Fractional Calculus

Antal Martinecz and Mihoko Niitsuma
Precision Mechanics, Chuo University, 1-13-27 Kasuga, Bunkyo-ku Tokyo 112-8551, Japan

Keywords: Image Processing, Retina, Fractional Calculus.

Abstract: The first part of a cone's signal transduction is investigated from an image processing perspective in order to find out what differentiates (human) vision from computer vision. We found that the activity of cone opsins—visual pigments that are activated by the impact of a photon—can be described as an approximation of a fractional integrator of order 0.1–0.2 on frequencies between 1–30 Hz. We explore how this affects the output signal and provide examples of how this can be used for noise reduction and image processing. We also present a simplified model since these processes require excessive computational power for computer vision modeling.

1 INTRODUCTION

Human vision is so reliable that it can override all other senses when conflicting inputs are presented; however, the same cannot be said of computer vision. A number of papers draw inspiration from human vision image processing, most of which model the network of retinal cells or part of the brain (Bratkova et al., 2009; Gould et al., 2007; Eeckman, 1989; Means, 1992; Yang et al., 2013).

The goal of this paper is to explore signal formation within the retina's cones after the impact of a photon to see how it affects the resulting signal and any subsequent image processing. Because the set of equations that describe this process require excessive computational power, it is necessary to determine what characterizes these equations to simplify them successfully.

According to our results, the equations that describe the activity of cone opsins behave as a fractional integrator $I^{0.2}$ on frequencies between 1–30 Hz. This means that it acts as a first order system—a low pass filter—above 30 Hz, and signals above 1 Hz are attenuated as well to a lesser extent.

2 MODELING

2.1 Signal Transduction of the Cones

Signal transduction is the formation of a cell's signal in response to an external stimulus. A complete review of this process is beyond the scope of this paper, so only the relevant parts will be reviewed: the activation and inactivation of cone opsins.

Because it is difficult to directly measure concentrations within a cell, there are controversial parts of this process such as inactivation rates (Gross and Burns, 2010; Korenbrot, 2012b; Invergo et al., 2013a; Zhang, 1997) and the number of phosphorylation sites (Korenbrot, 2012a; Qu and Vondriska, 2009). Therefore, one of the goals of this study is to determine what kind of behavior is expected from these kinds of equations and processes.

2.1.1 Activation and Inactivation

The impact of a photon in a cone activates a visual pigment (VP). When active, VPs activate their corresponding G-proteins ("transducins"). The inactivation of an active VP (VP*) consists of several steps. First, multiple phosphorylations by a G-protein kinase (GPK) occur, where each phosphorylation halves its ability to activate nearby transducins (Adamus et al., 1993; De Palo et al., 2013; Invergo et al., 2013b; Reiter and Lefkowitz, 2006). Next, phosphorylated VP*s are inactivated by arrestin, the rate of which depends on how many times the VP* has been phosphorylated.

Inactivate VPs (VP^0s) still have activity between 5% and 50% compared to the previous stage (Ascano and Robinson, 2006; Sinha et al., 2014). Finally, the binding of arrestin targets VP^0s for internalization, i.e., recycling it back to its default state. During this

Martinecz A. and Niitsuma M..
Modeling the G-Protein Signaling of the Retina with Fractional Calculus.
DOI: 10.5220/0005515304810488
In *Proceedings of the 12th International Conference on Informatics in Control, Automation and Robotics* (ICINCO-2015), pages 481-488
ISBN: 978-989-758-122-9

process, its activity (as a "free-opsin") is reduced to nearly zero, approximately $2.5 \cdot 10^5$–10^6 times weaker than the activity of an unphosphorylated VP* (Cornwall and Fain, 1994; Lamb and Pugh, 2004; Fan et al., 2005). Based on the differences in spontaneous activities in cones and rods, this should be a higher value (Yau and Hardie, 2009).

An active transducin form a complex with an inactive phosphodiestarese (PDE) making it active as long as it is bound. Active transducins are inactivated by the RGS9 complex, which makes it dissociate from the PDE, thereby halting its activity.

2.1.2 Adaptation

Adaptation is mostly controlled by processes downstream; for example, by the concentration of Ca++ within the cell (Invergo et al., 2013b; Arshavsky and Burns, 2012). In this paper, we include the adaptation that affects the maximum rate of VP* phosphorylation (Korenbrot, 2012a). With higher inputs, the phosphorylation rate is decreased making the output even higher as shown in Fig. 1.

The values of the adaptation were determined separately for an impulse response and for a step response in (Korenbrot, 2012a). In our model, the adaptation is dependent on the number of active VP*s within the simulated cell, this adequately approximates both the impulse and step response adaptation of the model described in (Korenbrot, 2012a).

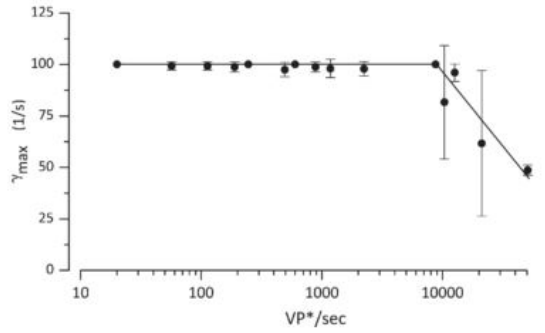

Figure 1: Adaptation of γ, depending on the number of VP*/sec on the input (step response version) (Korenbrot, 2012a).

2.1.3 Equations

We have opted to use the mathematical model of (Korenbrot, 2012b; Korenbrot, 2012a). Because of the range of possible parameters for VP^0 and free opsins in the literature, we have chosen not to extend the model to include them.

Let γ be the rate of phosphorylation; it's value ranges between 50 and 100 s^{-1} depending on adaptation. Furthermore, n_{PDE} is the number of active PDEs, the same as the number of active transducins in this model.

$$\dot{x_0} = \mathrm{input}(t) - \gamma \cdot x_0 \quad (1)$$
$$\dot{x_1} = \gamma \cdot x_0 - (\gamma \cdot 0.9 + 0.5)x_1 \quad (2)$$
$$\dot{x_2} = \gamma \cdot 0.9x_1 - (\gamma \cdot 0.9^2 + 2 \cdot 0.5)x_2 \quad (3)$$
$$\vdots$$
$$\dot{x_6} = (\gamma \cdot 0.9^5 + i \cdot 0.5)x_5 - 5 \cdot 0.5x_6. \quad (4)$$

The output (number of active PDEs) is:

$$\dot{n_{\mathrm{PDE}}} = 230(\sum_i 2^{-i}x_i) - 12.5 \cdot n_{\mathrm{PDE}}. \quad (5)$$

Arrestin binding is negligible with the exception of the state after the last phosphorylation since the phosphorylation is 20-fold faster. In steady state, each level of phosphorylation has 1.11 times more VP*s than the previous level, and since each successive level's activity is halved, they can be replaced with just one level with the activity of the first level and pole of the last phosphorylation. A comparison is shown in Fig. 2. The simplified model for six phosphorylation sites is:

$$\dot{x_0} = \mathrm{input}(t) - \gamma \cdot 0.9^6 \cdot x_0 \quad (6)$$
$$\dot{x_1} = \gamma \cdot 0.9^6 \cdot x_0 - 3x_1. \quad (7)$$

The output is:

$$\dot{n_{\mathrm{PDE}}} = 230(x_0 + 2^{-5}x_1) - 12.5n_{\mathrm{PDE}}. \quad (8)$$

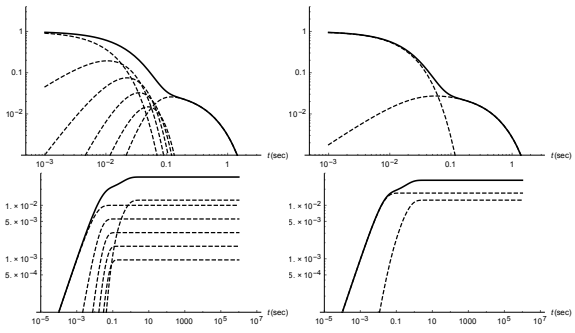

Figure 2: Impulse (top) and step (bottom) responses of the original (left) and simplified (right) models on a log–log scale. Solid curves represent the output, and dashed lines represent each feedback loop's contribution.

2.1.4 Range of Values

The time course from VP activation to VP* is negligible, specifically, it is 1 ms (Korenbrot, 2012b).

The lowest detectable values in cones can be produced by 4–10 unphosphorylated VP*s.

There are 10^8 VPs in a rod, so we assume that cones have a similar number of VPs (Lamb and Pugh, 2004). A flash of light activates 1–10^6 VP/sec (Korenbrot, 2012b).

This model does not address sensitivity loss due to the decrease of available VPs since the internalization process takes a considerable amount of time.

2.2 Fractional Calculus

Since the structure of this process is self-similar, we hypothesize that these equations describe a fractional integral (Charef et al., 1992; Clerc et al., 1984; Dalir and Bashour, 2010). In fractional calculus, instead of integer order integrals and derivatives (for example, I^1, I^5, D^2, D^{-13}), any order can be defined (for example, $I^{0.32}$, I^{π}, D^{4+2i}). In this paper, we restrict ourselves to the fractional integrals of a real order between 0 and 1.

An interpretation of a fractional integral is the distortion of the time scale during integration: time "slows down" as it approaches the present, therefore, giving it more weight (Podlubny, 2002). The opposite interpretation is that past values are being gradually "forgotten", and therefore, having less weight.

The Riemann-Liouville definition of the fractional integral is

$$\mathrm{I}^{\alpha} f(x) = \frac{1}{\Gamma(\alpha)} \int_a^b f(t)(b-t)^{\alpha-1} \mathrm{d}t. \qquad (9)$$

Using convolution, this can be converted to a more convenient form for those familiar with control theory:

$$\mathrm{I}^{\alpha} f(x) = \frac{1}{\Gamma(\alpha)} f(t) \otimes t^{\alpha-1}. \qquad (10)$$

If $0 < \alpha < 1$, the impulse response of a fractional integrator is $(1/t)^c$. Compared to a feedback loop's exponential e^{-t} on a logarithmic scale, the slope of the function does not change over the logarithm of time; therefore, the time it takes for the signal to be undetectable greatly depends on the input signal's strength (see Fig. 3).

2.2.1 Approximation

Since as an operation the fractional integral is linear, it can be approximated by approximating its impulse response. The gamma function from a signal processing standpoint is just a gain for the whole operation therefore it can be neglected. In order to show that the equations that describe the activity of cone opsins act as a fractional integral, it suffices to show that a fractional integral's impulse response is approximated by the system.

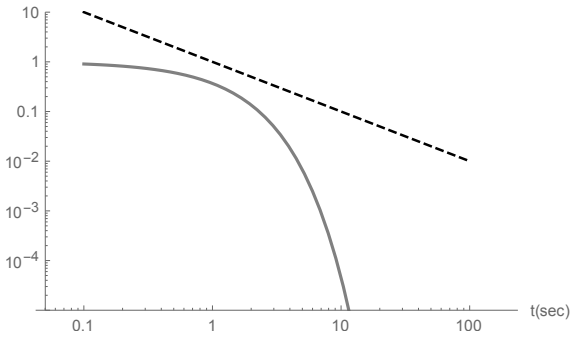

Figure 3: Exponential decay ($g(t) = e^{-t}$, solid curve) and power-law decay ($f(t) = 1/t$, dashed line) on a log–log plot.

In log–log scale, its impulse response is linear; therefore, it can be approximated by a piecewise constant function. For example, signals that occur

- 0.1–1 s ago have an average weight $\sim 0.3^{\alpha-1}$,
- 1–10 s ago have an average weight $\sim 3^{\alpha-1}$,
- 10–100 s ago have an average weight $\sim 30^{\alpha-1}$,

and so on, where α is the order of the fractional integral (see Fig. 4).

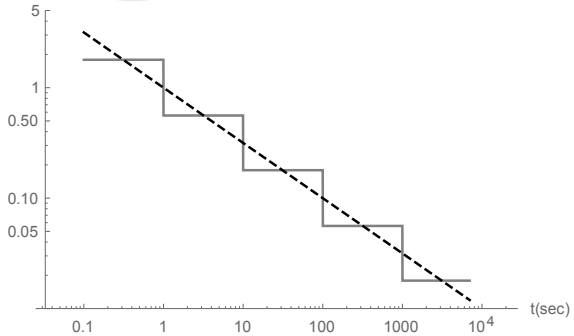

Figure 4: Piecewise approximation (solid lines) of $f(t) = t^{-0.5}$ (dashed) on a log–log plot.

Connected feedback loops form similar groups to the piecewise function mentioned above. This also reduces the necessary memory for the operation to only a few variables, even on extended timescales such as minutes.

With differential equations:

$$\dot{x_0} = \mathrm{input}(t) - ax_0 \qquad (11)$$
$$\dot{x_1} = ax_0 - bx_1 \qquad (12)$$
$$\dot{x_2} = bx_1 - cx_2 \qquad (13)$$
$$\vdots$$

The output is the weighted sum of x_i:

$$y = \sum_i (c_i x_i). \tag{14}$$

Since we want to exploit the self-similar nature of this model on the log–log plot, the poles of the feedback loops have to decrease logarithmically (100, 10, 1, ..., etc.), or at least it has to be self-affine (100, 8, 1.5, ..., etc.).

A feedback loop's settling time is 3–4 times its time constant depending on the definition used: within 5% or 2% of the final value. We assume the *i*th loop receives an impulse input at $t = 0$ and has a time constant of $\tau_i = 1$. If the next loop's time constant $\tau_{i+1} \gg \tau_i$, the maximum of the next loop will be between approximately $2\tau_i$ and $3\tau_i$.

If $\tau_{i+1} = 10\tau_i$, to find the lower bound of x_{i+1}'s maximum, the following approximation is used: at $t = 0$, it receives all the inputs it would receive until its maximum: $t = 2\tau_i ... 3\tau_i$. While this ignores the fact that x_{i+1} is gradually filled, it is a good estimate for finding the time it reaches its maximum.

$$x_{i+1}(0) = 1 - x_i(2...3\tau_i). \tag{15}$$

The maximum is at $t = 2.5\tau_i$, where the second loop is at least 71.5% full (maximum is at $2.5\tau_i$):

$$x_{i+1}(2.5\tau_i) \approx (1 - e^{-2.5}) \cdot e^{-2.5/10} = 0.7148. \tag{16}$$

While this may be below the desired value, the influence of the previous loop will still have an effect on the output as shown in Fig. 5. After $3\tau_i$, the *i+1*st loop receives little to no input from the previous loop and decays exponentially in the same manner as the *i*th loop. Since the system is self-affine, the *i+2*nd loop can be calculated the same way.

The weight of each loop depends on the maximum of each loop's impulse response. To approximate a fractional integral, the maximums have to form a line on the log–log plot.

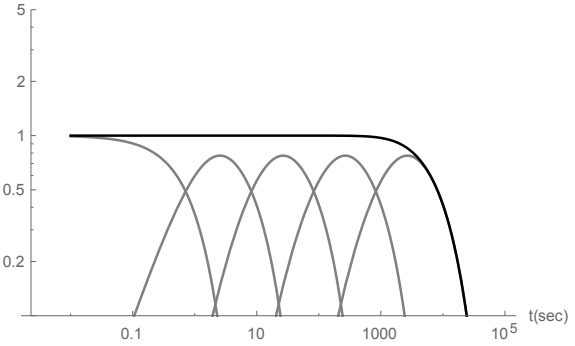

Figure 5: Approximation without different weights on the log–log plot. Gray lines represent the contribution of each loop, and the black curve is the output.

$$\log \frac{c_i}{c_{i-1}} = (\alpha - 1) \log \frac{t_{\max,i}}{t_{\max,i-1}}, \tag{17}$$

where α is the order of integration, and $t_{\max,i}$ is the time to each loop's peak.

Assuming that the next loop's maximum is $x \cdot \tau_i$ (some multiple of τ):

$$t_{\max,i} \approx x \sum_{k=0}^{i} \tau_k. \tag{18}$$

For even logarithmic spacing ($\tau_i = \tau_0^i$), the maximums form a geometric series:

$$t_{\max,i} \approx x \sum_{k=0}^{i} \tau_k = x \frac{1 - \tau_0^{(i+1)}}{1 - \tau_0}. \tag{19}$$

Hence, (17) can be rewritten as

$$\log \frac{c_i}{c_{i-1}} = (\alpha - 1) \log \frac{1 - \tau_0^{(i+1)}}{1 - \tau_0^i}. \tag{20}$$

In other words, the approximation is independent of x (the relative place of the maximums).

If $\tau_0 \geq 5$ and $\tau_i = \tau_0^i$, the displacement of the maximums can be neglected as well:

$$\log \frac{c_i}{c_{i-1}} \approx (\alpha - 1). \tag{21}$$

Overall, if the poles are sufficiently far and spaced logarithmically, then the *i*th loop's pole and gain will dominate the given impulse response on its timescale.

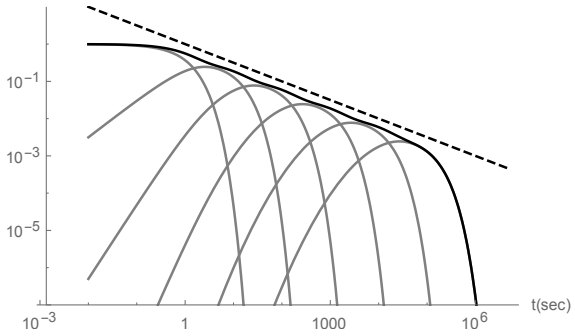

Figure 6: Approximation of $f(t) = t^{-0.5}$ with feedback loops on the log–log plot. Gray lines represent the contribution of each loop, and the black curve is the output.

3 RESULTS

3.1 Approximation Example

Consider the approximation of I^α where the poles are $p_i = 10^i$ and five feedback loops are used (the bare minimum is two loops). Strictly speaking $\Gamma(\alpha) \cdot I^\alpha$,

since for signal processing the gamma function was neglected. The state space representation is:

$$A = \begin{bmatrix} -1 & 0 & 0 & 0 & 0 \\ 1 & -0.1 & 0 & 0 & 0 \\ 0 & 0.1 & -0.01 & 0 & 0 \\ 0 & 0 & 0.01 & -0.001 & 0 \\ 0 & 0 & 0 & 0.001 & -0.0001 \end{bmatrix}$$

$$B = \begin{bmatrix} 1 & 0 & 0 & 0 & 0 \end{bmatrix}^{\mathrm{T}}$$

$$C = \begin{bmatrix} 1 & 0.1^{\alpha-1} & 0.1^{2(\alpha-1)} & 0.1^{3(\alpha-1)} & 0.1^{4(\alpha-1)} \end{bmatrix}.$$

The Bode plots of fractional integrals have a slope of -20α dB/dec and a constant phase of -90α deg (Podlubny et al., 2002; Sierociuk et al., 2013). Both Bode plots and impulse responses fully define a linear time invariant system.

In case of the approximation as α approaches zero (the identity operation), the approximation gets less and less reliable. The algorithm works for $\alpha > 1$ as well; however, outside the chosen frequency band, the system behaves as a first-order system not as $\lceil\alpha\rceil$ as shown in Fig. 7.

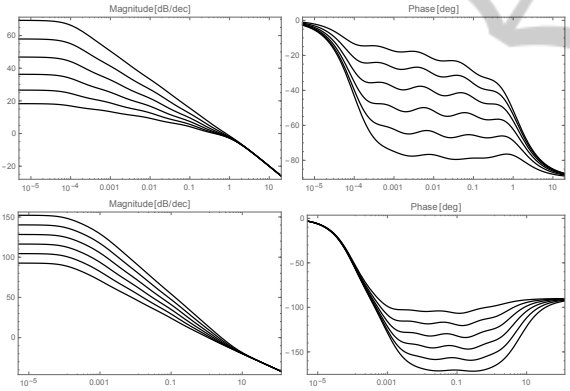

Figure 7: Bode plots of the approximations of $I^{0.15}$, $I^{0.3}$, $I^{0.45}$, $I^{0.6}$, $I^{0.75}$, $I^{0.9}$ (top) and $I^{1.15}$, $I^{1.3}$, $I^{1.45}$, $I^{1.6}$, $I^{1.75}$, $I^{1.9}$ (bottom).

Note that imperfect data transfer has a similar effect to having reduced weights since it will reduce the gain of the subsequent loops.

3.2 Signaling of Cone Opsins

We have shown that the signaling of cone opsins in Eq. (6) and (7) can approximate a fractional integral; in particular, they describe an approximation with an order of 0.2 between 1–30 Hz as shown in Fig. 8.

An extended model involving VP^0s and free opsins also fits the approximation on a broader range between 0.1–30 Hz with an order of 0.1 (depending on the values used). However, it is difficult to prove which values are appropriate without further comparison to biological data; therefore, we have chosen not to include it in our demonstrations for now.

This kind of power-law behavior in cells is not unheard of; for example, it is theorized that there is a power-law component of the auditory nerves' adaptation (Zilany and Carney, 2010). The activity of vestibulo-oculomotor neurons is described with fractional calculus in (Anastasio, 1994; Thorson and Biederman-Thorson, 1974).

To see how power-law behavior affects video input, simulations were conducted using Wolfram-Mathematica 10 and the nVidia CUDA framework. The simplified cone equations with adaptation included were simulated for each cell. Based on step responses, the output image was determined to be the sum of the following two images with different weights depending on adaptation:

- imageA: an image that is almost the same as one frame from a 30 Hz camera,
- imageB: an image that is the sum of the past approximately 30 frames.

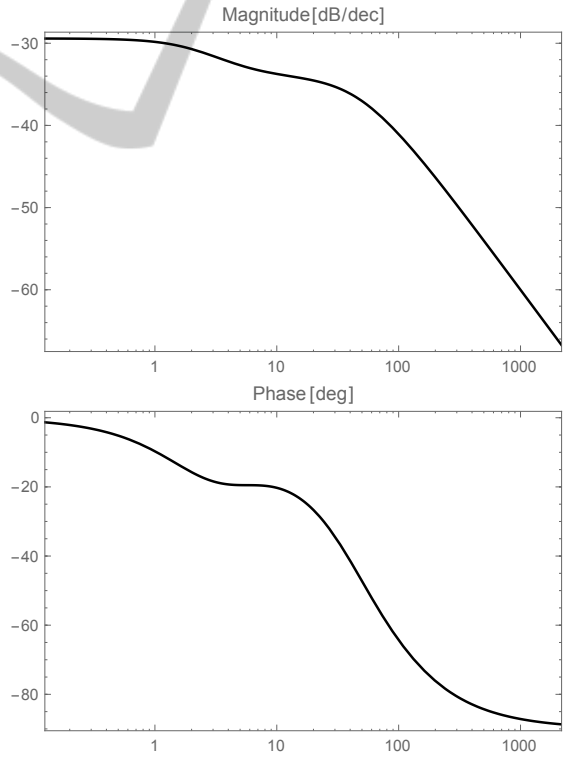

Figure 8: Bode plots of the simplified model ($\gamma = 100\ \mathrm{s}^{-1}$). Note the constant phase around 18 deg.

3.3 Image Processing

As input, a game and movie trailer were used: the "Harry Potter: Half-Blood Prince" trailer and the "World of Warcraft: Wrath of the Litch King" trailer. Both have eye tracking data available at (Mital et al., 2011) for later parts of research.

It should be kept in mind during the evaluation that eye movements have unique properties; specifically, they are characterized as "ballistic": fast movements followed by short stops. As a natural mechanism, the eyes tend to focus on certain points of moving objects, which means that the scene in focus should only change by 2–5 Hz. This has not been modeled at this stage of our research.

3.4 Noise Reduction

Assuming a Gaussian distribution of temporal noise, unlike imageA, imageB contains little to no noise. For example, refer to the snowflakes in Fig. 9. A feedback loop as a low-pass filter for noise reduction is inefficient because quickly moving parts are blurred and often "invisible", however in the case of the fractional integral they can still be detected because of imageA as shown in Fig. 10.

The adaptive process changes the ratio of imageA and imageB by increasing the lifetime of VP^0s for stronger inputs. This means that brighter scenes (and pixels) have less noise reduction. The effects of the non-linearity produced by this adaptation are difficult to detect. Similarly to a camera, darker scenes would contain more noise otherwise. The bright areas become 50% brighter; however, after scaling back the values between 0–255 for display and print purposes, the introduced non-linearity becomes invisible, see Fig. 10.

3.5 Partially Obstructed Images

As a special case, in the Harry Potter trailer, there is a scene where he runs in tall grass. Since the camera follows him, it is similar to simulated eye movement (however, vertical movement is not stabilized). On multiple frames, his face is partially obstructed by leaves, so an object or face recognition algorithm may be difficult to apply. However, because of imageB, there is a faint outline of his face that remains from previous frames as can be seen in Fig. 11. While this is is an unusual problem, we believe that it is representative of the flexibility of human vision.

Figure 9: Scene from the World of Warcraft trailer (top). After processing (with adaptation), the same snowfall is barely visible (bottom).

Figure 10: Scene from the World of Warcraft trailer (top). With adaptation, compared to the original, there is little to no difference in the brightness values (bottom).

4 FUTURE DIRECTIONS

There are two directions this research will take: eye movements and investigating the full model of cones.

4.1 Patterns

In (Sligte et al., 2008), it is hypothesized that there

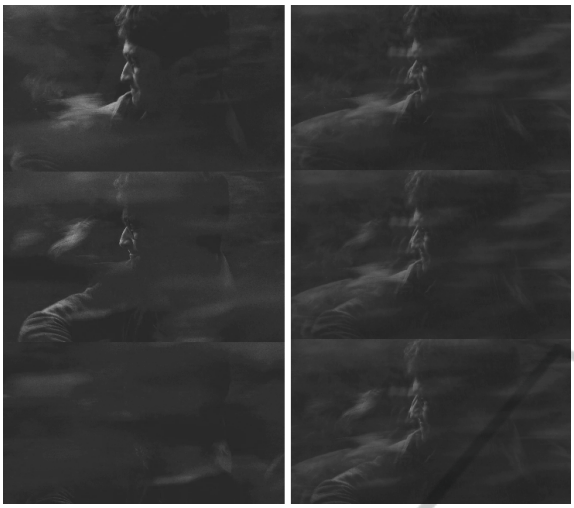

Figure 11: Three frames from the original Harry Potter trailer (left column). After processing—because of the afterimage—parts of his face are no longer obstructed by leaves (right column).

are three visual short-term memory storages. Of the three, short-term iconic memory is most relevant to this paper since it stores visual information in positive afterimages for brief periods of time. There is a distinction between rods and cones; rods provide a stronger afterimage because of their slow response (there is basically only imageB). This type of memory has been tested by them using different masking images to erase the afterimage provided by the cones, leaving the afterimage provided by the rods and vice-versa. Short-term iconic memory is weaker in cones although still present. This is consistent with our findings, as cones still provide a weak but noticeable afterimage. Eye movements will be used in later parts of our research to assess their basic function and potential for image processing.

For finding breaks in a pattern, it is the easiest to subtract two subsequent frame; however in biological systems this operation is a bit more difficult. Our hypothesis is that since eye movements cannot instantaneously compare two images by subtraction, buffering the previous frame is not enough since it only contains data about eye movements. Moreover, it is not known when and what information will be useful in the future, so storing a second of data in imageB makes the most sense. For this operation a substantial overshoot is needed in the next processing steps. Bipolar cells for example are the next row of cells after cones and rods and get the cones' output as input. Their impulse responses substantially overshoot, so any difference between imageA and imageB will be highlighted (Ichinose et al., 2014; Wassle, 2004).

4.2 Curves, Parallel Lines

When focusing on lines (edges), the eyes will focus on the points of the line instead of focusing on an empty space next to the line. When changing focus from one point to another on the line, an overshoot in the subsequent processing steps will highlight the differences between imageA and imageB. Therefore it will be very apparent if the line is not completely straight or if nearby edges/lines are not parallel.

5 CONCLUSIONS

There is a difference between the data processing of the retina and traditional computer-based image processing; the retina has video processing, and individual cones and rods process input as a function of time. Moreover, the network of cones affect each other, and their output depend on all the values of the past minute (as well as the horizontal, amacrine, bipolar, and ganglion cells downstream). We have shown how this affects video input and how it might be utilized by our eyes. We also discussed why eye movements are important and how they affect this kind of processing. Based on our findings, we believe that processing a video as a whole instead of frame-by-frame has great potential.

REFERENCES

Adamus, G., Arendt, A., Hargrave, P. A., Heyduk, T., and Palczewski, K. (1993). The kinetics of multiphosphorylation of rhodopsin. *Archives of biochemistry and biophysics*, 304(2):443–7.

Anastasio, T. J. (1994). The fractional-order dynamics of brainstem vestibulo-oculomotor neurons. *Biological cybernetics*, 72(1):69–79.

Arshavsky, V. Y. and Burns, M. E. (2012). Photoreceptor signaling: supporting vision across a wide range of light intensities. *The Journal of biological chemistry*, 287(3):1620–6.

Ascano, M. and Robinson, P. R. (2006). Differential phosphorylation of the rhodopsin cytoplasmic tail mediates the binding of arrestin and its splice variant, p44. *Biochemistry*, 45:2398–2407.

Bratkova, M., Boulos, S., and Shirley, P. (2009). oRGB: a practical opponent color space for computer graphics. *IEEE computer graphics and applications*, 29(1):42–55.

Charef, A., Sun, H., Tsao, Y., and Onaral, B. (1992). Fractal system as represented by singularity function. *IEEE Transactions on Automatic Control*, 37(9):1465–1470.

Clerc, J., Tremblay, A.-M., Albinet, G., and Mitescu, C. (1984). a.c. response of fractal networks. *Journal de Physique Lettres*, 45(19):913–924.

Cornwall, M. C. and Fain, G. L. (1994). Bleached pigment activates transduction in isolated rods of the salamander retina. *The Journal of physiology*, 480 (Pt 2:261–79.

Dalir, M. and Bashour, M. (2010). Applications of fractional calculus. *Applied Mathematical Sciences*, 4(21):1021–1032.

De Palo, G., Facchetti, G., Mazzolini, M., Menini, A., Torre, V., and Altafini, C. (2013). Common dynamical features of sensory adaptation in photoreceptors and olfactory sensory neurons. *Scientific reports*, 3:1251.

Eeckman, F. (1989). A retina-like model for motion detection. In *International Joint Conference on Neural Networks*, pages 247–249 vol.2. IEEE.

Fan, J., Woodruff, M. L., Cilluffo, M. C., Crouch, R. K., and Fain, G. L. (2005). Opsin activation of transduction in the rods of dark-reared Rpe65 knockout mice. *The Journal of physiology*, 568(Pt 1):83–95.

Gould, S., Arfvidsson, J., Kaehler, A., Sapp, B., Messner, M., Bradski, G., Baumstarck, P., Chung, S., and Ng, A. Y. (2007). Peripheral-foveal vision for real-time object recognition and tracking in video. In *International Joint Conference on Artificial Intelligence*, pages 2115–2121. Morgan Kaufmann Publishers Inc.

Gross, O. P. and Burns, M. E. (2010). Control of rhodopsin's active lifetime by arrestin-1 expression in mammalian rods. *The Journal of neuroscience : the official journal of the Society for Neuroscience*, 30(9):3450–7.

Ichinose, T., Fyk-Kolodziej, B., and Cohn, J. (2014). Roles of ON Cone Bipolar Cell Subtypes in Temporal Coding in the Mouse Retina. *Journal of Neuroscience*, 34(26):8761–8771.

Invergo, B. M., Montanucci, L., Koch, K.-W., Bertranpetit, J., and Dell'orco, D. (2013a). Exploring the rate-limiting steps in visual phototransduction recovery by bottom-up kinetic modeling. *Cell communication and signaling : CCS*, 11(1):36.

Invergo, B. M., Montanucci, L., Laayouni, H., and Bertranpetit, J. (2013b). A system-level, molecular evolutionary analysis of mammalian phototransduction. *BMC evolutionary biology*, 13:52.

Korenbrot, J. I. (2012a). Speed, adaptation, and stability of the response to light in cone photoreceptors: the functional role of Ca-dependent modulation of ligand sensitivity in cGMP-gated ion channels. *The Journal of general physiology*, 139(1):31–56.

Korenbrot, J. I. (2012b). Speed, sensitivity, and stability of the light response in rod and cone photoreceptors: Facts and models. *Progress in retinal and eye research*, 31(5):442–466.

Lamb, T. D. and Pugh, E. N. (2004). Dark adaptation and the retinoid cycle of vision. *Progress in retinal and eye research*, 23(3):307–80.

Means, R. (1992). Neural Network Retinal Model Real Time Implementation.

Mital, P. K., Smith, T. J., Hill, R., and Henderson, J. M. (2011). Clustering of gaze during dynamic scene viewing is predicted by motion. *Cognitive Computation*, 3(1):5–24.

Podlubny, I. (2002). Geometric and Physical Interpretation of Fractional Integration and Fractional Differentiation. *Fractional Calculus and Applied Analysis*, 5(4):367–386.

Podlubny, I., Petraš, I., and Vinagre, B. (2002). Analogue realizations of fractional-order controllers. *Nonlinear dynamics*, pages 281–296.

Qu, Z. and Vondriska, T. M. (2009). The effects of cascade length, kinetics and feedback loops on biological signal transduction dynamics in a simplified cascade model. *Physical biology*, 6(1):016007.

Reiter, E. and Lefkowitz, R. J. (2006). GRKs and beta-arrestins: roles in receptor silencing, trafficking and signaling. *Trends in endocrinology and metabolism: TEM*, 17(4):159–65.

Sierociuk, D., Podlubny, I., and Petras, I. (2013). Experimental Evidence of Variable-Order Behavior of Ladders and Nested Ladders. *IEEE Transactions on Control Systems Technology*, 21(2):459–466.

Sinha, A., Jones Brunette, A. M., Fay, J. F., Schafer, C. T., and Farrens, D. L. (2014). Rhodopsin TM6 can interact with two separate and distinct sites on arrestin: Evidence for structural plasticity and multiple docking modes in arrestin-rhodopsin binding. *Biochemistry*, 53:3294–3307.

Sligte, I. G., Scholte, H. S., and Lamme, V. a. F. (2008). Are there multiple visual short-term memory stores? *PloS one*, 3(2):e1699.

Thorson, J. and Biederman-Thorson, M. (1974). Distributed relaxation processes in sensory adaptation. *Science (New York, N.Y.)*, 183(4121):161–72.

Wassle, H. (2004). Parallel processing in the mammalian retina. *Nature reviews. Neuroscience*, 5(October):747–757.

Yang, K., Gao, S., Li, C., and Li, Y. (2013). Efficient Color Boundary Detection with Color-Opponent Mechanisms. *2013 IEEE Conference on Computer Vision and Pattern Recognition*, pages 2810–2817.

Yau, K. and Hardie, R. (2009). Phototransduction motifs and variations. *Cell*, 139(2):246–264.

Zhang, L. (1997). Rhodopsin Phosphorylation Sites and Their Role in Arrestin Binding. *Journal of Biological Chemistry*, 272(23):14762–14768.

Zilany, M. S. a. and Carney, L. H. (2010). Power-law dynamics in an auditory-nerve model can account for neural adaptation to sound-level statistics. *The Journal of neuroscience*, 30(31):10380–90.